



Computational Fluid Dynamics Analysis of Drag Reduction in Bullet via Geometric Modifications

Hacımurat DEMİR^{1*} , Mehmet ÇİMEN¹ , Ömer YILMAN¹ , Erhan TEKİN¹ 

¹Aksaray University, Department of Mechanical Engineering, 68100, Aksaray, Turkey

Keywords:

Bullet,
Ballistics,
Compressible flow,
CFD,
Drag coefficient

Abstract

In the field of external ballistics, the geometry (shape and structure) of the projectile plays a significant role. This geometry affects a multitude of variables, including air resistance, stability, range, and accuracy. The objective of this study was to decrease the drag coefficients by making different geometric alterations to the Spitzer-type ogive bullet and examining the flow conditions, Mach number, and pressure distributions around the projectile using a three-dimensional numerical simulation. Upon examination of the results, it was observed that the flow exhibited subsonic stagnation zones and a velocity drop upstream of the nose tip. The flow became slightly supersonic as it expanded around the ogive nose and boattail junction. Expansion fans and recompression shocks were detected at the points where the ogive-shaped nose of the projectile transitions to the body, where the boattail-shaped rear of the projectile transitions to the body, and at the base of the projectile. The pressure coefficient value reached its maximum value of $C_p=0.7$ when the air decelerated and dropped to $C_p=-0.5$ as the projectile transitioned from the nose to the body. A gradual decrease in pressure along the projectile surface resulted in a more consistent and lower pressure coefficient compared to the nose. The A3-type bullet, including the most extensive spiral groove, exhibited a 12.4% enhancement in drag reduction as compared to the original bullet. The B-series of straight grooves exhibited a considerable decrease in drag. Nevertheless, the efficacy of helical grooves in regulating flow separation at the tail surpassed that of other methods. The A-series bullets, namely A2 and A3, were well-suited for applications that demanded little aerodynamic resistance. The B-series bullets exhibited enhancements compared to the conventional design and may be deemed suitable for more straightforward production or design limitations.

*e-mail: hmdemir@aksaray.edu.tr

Bu makaleye atıf yapmak için:

Hacımurat DEMİR; Mehmet ÇİMEN; Ömer YILMAN; Erhan TEKİN, "Computational Fluid Dynamics Analysis of Drag Reduction in Bullet via Geometric Modifications", Bayburt Üniversitesi Fen Bilimleri Dergisi, C. 7, s 1, ss. 47-56

How to cite this article:








Hacımurat DEMİR; Mehmet ÇİMEN; Ömer YILMAN; Erhan TEKİN, "Computational Fluid Dynamics Analysis of Drag Reduction in Bullet via Geometric Modifications", Bayburt University Journal of Science, vol. 7, no 1, pp. 47-56

1 INTRODUCTION

A bullet is defined as a component of a firearm cartridge that is ejected from the barrel during the firing process. Different components and designs determine the performance and intended use of bullets. The bullet's core, case, shell, powder, and capsule shape the bullet's ballistic properties and its effects on the target. The classification of bullets is based on their intended use and design. Table 1 below shows some of the most common bullet types. Additionally, ballistics is a scientific discipline that investigates the movement, characteristics, and effects of projectiles, including bullets, rockets, missiles, and any other objects launched into the atmosphere or outer space. It covers various disciplines, including engineering, mathematics, physics, and material science, to understand how bullets move in the air or other environments and how they interact with targets upon impact. Ballistics may be categorized into three main classifications:

- Internal ballistics
- External ballistics
- Terminal ballistics

Table 1. Types of bullets

Full Metal Jacket (FMJ)	Round Nose	
	Boat Tail	
Hollow Point (HP)	Boat Tail	
Soft Point (SP)	Flat Nose	
	Round Nose	
	Flat Base Spitzer	
	Boat Tail Spitzer	

Internal ballistics concerns the propulsion of the projectile; external ballistics describes the projectile's atmospheric flight; and terminal ballistics is concerned with the impact of the projectile on the target. Modern external ballistics is a specialized branch of the dynamics of rigid bodies moving under the influence of gravitational and aerodynamic forces. In general, external ballistics concerns the trajectory of a bullet from the barrel of a gun to its intended target. The flow environment surrounding the rifle demonstrates the effect on the projectile. In order to prevent misdirection of the shooting trajectory, it is a necessity to analyze the aerodynamic coefficients acting on the surface of the projectile, such as lift, drag, and momentum [1, 2].

It is important to consider the drag coefficient when analyzing external ballistics. For example, a 130 mm artillery shell at 943 m/s in a vacuum has a maximum range of 90.7 km; however, this reduces to 24 km in the presence of air. Therefore, the drag coefficient plays a vital role in determining range, with the shape of the projectile having a significant influence [3]. When analyzing the relevant research in the literature within this perspective, Ferfour et al. [2] examined the overall drag coefficient of the 155mm M107 axisymmetric projectile in axisymmetric flow without any yaw. They stated that an analysis of various drag components, including base drag, pressure drag, and friction drag, allowed for the assessment of their respective impacts on total drag, considering the Mach number and flow conditions.

Sahoo and Laha [3] conducted a study to analyze the changes in drag and estimate the trajectory elements of a 130 mm artillery shell with two distinct nose shapes. The study attempted to find the coefficient of drag and shock wave pattern exhibited by the shell when moving through a supersonic airflow with no angle of attack. A positive correlation was found between the drag coefficient, the presence of a detached shock wave, and an increase in the radius of the shell nose. Gholap et al. [4] studied the impact of wall proximity on an AK 47 bullet moving at $Ma=2$, analyzing how the heights influenced the flowfield, pressure distributions, aerodynamic coefficients, and wake region. They found that when the bullet was close to the wall, flow separation was minimal, limiting the formation of the bow shock wave. As the bullet's height increased, the bow shock wave formed and interacted with the

separating shock, increasing drag. Similarly, Selimli [5] investigated the contribution of improvements in bullet geometries to bullet range and target stabilization. They examined the effect of dimple and riblet structures on the 9 mm diameter parabellum-type bullet core model using ANSYS Design Modeler software. The results showed that both structures decreased drag force and shear stress on the projectile shape while enhancing airflow speed. Reddy et al. [6] performed computational simulations utilizing ANSYS-FLUENT to examine the drag coefficient of 155 mm artillery projectiles with and without base bleed. The study employed a density-based algorithm and utilized the $k-\omega$ SST turbulence model to analyze turbulent stresses. The findings indicated a 14.4% decrease in drag coefficient when using base bleed with an angle of attack of 0° . In a related study, Khan et al. [7] examined the variables that influence the lift and drag forces on bullets by utilizing Ansys Fluent. The findings indicated that the size of the bullet and the angle of attack were vital factors in determining the drag force. It was discovered that increasing the length and angle of attack of the bullet had a substantial impact on the drag force and lift forces, thereby influencing both the accuracy and penetrating power.

Moreover, Gan [8] conducted a study to determine the drag coefficients of various projectile geometries at low and high velocities. The findings indicated that the presence of riflings on the projectiles' surfaces did not have a substantial impact on the drag force generated by the pressure differential. Similarly, the intricate flow within hollow spaces did not have a significant influence on the outcomes. Furthermore, Salunke et al. [9] conducted a study on the characteristics of three bullets used in firearms: the NATO 5.56 mm bullet, the APM2's 7.62 mm bullet, and the AK-47 7.82 mm bullet. They found that the APM2 bullet had the highest level of drag, followed by the AK-47 7.82 mm bullet and the 5.56 mm bullet. The 7.82 mm bullet reached its maximum lifting force at a diameter to height ratio of 1.0. On the other hand, Serdarevic-Kadic and Terzic [10] conducted numerical simulations to examine the impact of base shape on a projectile's drag coefficient at transonic and supersonic speeds. They found that the base drag component, which is caused by the projectile's base shape, contributed up to 50% or more of the total drag, and reducing this drag increased the projectile's range.

In this study, a three-dimensional numerical simulation was conducted to reduce the drag coefficients by implementing a series of geometric modifications to the Spitzer-type ogive bullet. The ANSYS Fluent software was employed for numerical modeling, with the objective of investigating the drag coefficient on the projectile and the flow conditions, velocity, and pressure distributions around the projectile under the condition of a constant Mach number of 1. The findings of the study provide a comparison of different groove structures in terms of aerodynamic efficiency and performance. The objective is to identify the optimal groove structure that will enhance performance by reducing aerodynamic resistance in ammunition design.

2 COMPUTATIONAL METHODS

2.1 Model geometry

In this study, a typical tangent-type Spitzer bullet was selected due to its well-defined projectile geometry and its increasing use in numerous applications [11]. The geometry of the bullet was derived from the study by Larson et al. [12]. The bullet's geometries were designed using SolidWorks. While making alterations to the geometry of the existing bullet model, care was taken to preserve the length of the model and its middle section. This approach reflects the intention to maintain geometric balance on the bullet. As depicted in Figure 1, the influence of the length of the helical groove created on the bullet was initially examined. Additionally, in Figure 2, the effect of the length of the straight groove created in the bullet's tail section was also assessed. The geometries created in SolidWorks were imported into ANSYS Fluent in order to execute the planned simulations.

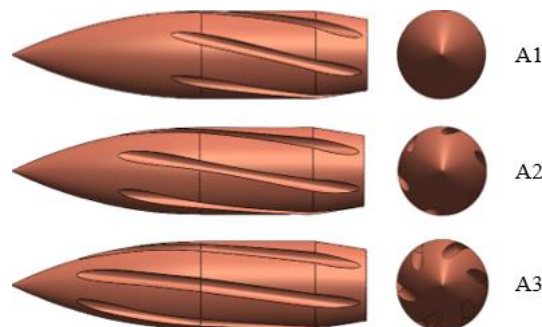


Figure 1. The geometry of bullets designed with increased helical modifications

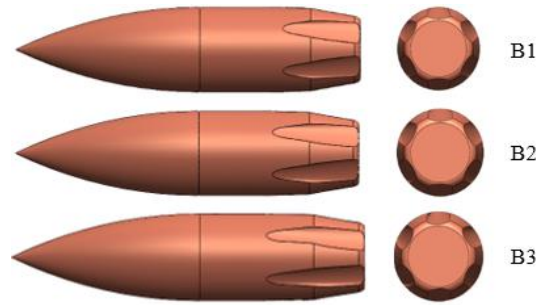


Figure 2. The geometry of bullets designed with increased aperture at the rear

2.2 Computational solver and governing equations

A three-dimensional, steady-state solution has been achieved by implementing an implicit density-based solver. The fluid material used is air, with the density set at ideal gas, and a three coefficient Sutherland viscosity method has been employed. The Spalart-Allmaras (SA) turbulence model was employed to simulate the airflow around the bullet. The single-equation SA turbulence model is chosen for this work because of its extensive usage in analyzing compressible outflow circumstances, particularly in high Reynolds number outflow issues, and its computational efficiency. The computations were conducted for a constant Mach number of 1. A second-order upwind scheme and an implicit formulation with a Roe-Finite Difference Scheme (Roe-FDS) were used to calculate the convective and pressure fluxes, thereby improving the accuracy of numerical calculations. The Green Gauss cell-based approach was used for spatial discretization, and the results were looked at when the residual convergence dropped below 10^{-4} .

The Navier-Stokes equations, often called the N-S equations, are the equations that explain the natural phenomena that occur in a continuum medium. It is possible to formulate them in tensor form ($i=1, 2, \text{ and } 3$) using the differential formulation, which is as follows:

- Conservation of the mass: $\frac{\partial \rho}{\partial t} + \frac{\partial}{\partial x_i}(\rho u_i) = 0$ (1)

- Conservation of the momentum: $\frac{\partial}{\partial t}(\rho u_i) + \frac{\partial}{\partial x_j}(\rho u_i u_j) = -\frac{\partial p}{\partial x_i} + \frac{\partial \sigma_{ij}}{\partial x_j}$ (2)

- Conservation of energy: $\frac{\partial}{\partial t} \rho \left(e + \frac{1}{2} u_i u_i \right) + \frac{\partial}{\partial x_j} \left[\rho u_j \left(h + \frac{1}{2} u_i u_i \right) \right] = \frac{\partial}{\partial x_j} (\sigma_{ij} u_i) - \frac{\partial q_j}{\partial x_j}$ (3)

where ρ is the density, u_i is the i th component of the velocity vector, x_i is the i th component of the position vector, p is the pressure, e is the specific internal energy, and h is the specific enthalpy. Furthermore, q_j j th component of the heat flux vector and σ_{ij} is the stress tensor, which is of second order and symmetric [13].

Transport equation for the SA turbulence model is given by the Eqn. 4:

$$\frac{\partial}{\partial t}(\rho \tilde{v}) + \frac{\partial}{\partial x_j}(\rho \tilde{v} u_j) = G_v + \frac{1}{\sigma_v} \left[\frac{\partial}{\partial x_j} \left\{ (\mu + \rho \tilde{v}) \frac{\partial \tilde{v}}{\partial x_j} \right\} + C_{b2} \rho \left(\frac{\partial \tilde{v}}{\partial x_j} \right)^2 \right] - Y_v + S_v$$
 (4)

The turbulent viscosity, μ_t is computed as it is given in Eqn. 5:

$$\mu_t = \rho \tilde{v} f_{v1}$$
 (5)

In Eqn. 5, f_{v1} denotes the viscous damping function and given by

$$f_{v1} = \frac{\chi^3}{\chi^3 + C_{v1}^3} \quad \text{with } \chi \equiv \frac{\tilde{v}}{\nu}$$
 (6)

The production term, G_v is modeled as:

$$G_v = C_{b1} \rho \tilde{S} \tilde{v} \quad (7)$$

$$\text{where } \tilde{S} \equiv S + \frac{\tilde{v}}{\kappa^2 d^2} f_{v2} \quad (8)$$

$$\text{and } f_{v2} = 1 - \frac{\chi}{1 + \chi f_{v1}} \quad (9)$$

C_{b1} and κ are constants, S is a scalar measure of the deformation tensor and d is the distance from the wall. As in the original model proposed by Spalart and Allmaras, S is determined by the vorticity's magnitude in ANSYS FLUENT by default [14]:

$$S \equiv \sqrt{2\Omega_{ij}\Omega_{ij}} \quad (10)$$

where Ω_{ij} is the mean rate-of-rotation tensor and is defined by:

$$\Omega_{ij} = \frac{1}{2} \left(\frac{\partial u_i}{\partial x_j} - \frac{\partial u_j}{\partial x_i} \right) \quad (11)$$

The destruction term is modeled as:

$$Y_v = C_{\omega1} \rho f_{\omega} \left(\frac{\tilde{v}}{d} \right)^2 \text{ and } f_{\omega} = g \left[\frac{1 + C_{\omega3}^6}{g^6 + C_{\omega3}^6} \right]^{1/6} \quad (12)$$

$$\text{where } g = r + C_{\omega2} (r^6 - r) \text{ and } r \equiv \frac{\tilde{v}}{\tilde{S} \kappa^2 d^2} \quad (13)$$

$C_{\omega1}$, $C_{\omega2}$, and $C_{\omega3}$ are constants, and \tilde{S} is given by Eqn. 8. Note that the modification described above to include the effects of mean strain on S will also affect the value of \tilde{S} used to compute r . The model constants have the following default values [15]:

Table 2. The values of model constants

Constant	Value	Constant	Value
κ	= 0.4187	C_{v1}	= 7.1
$\sigma_{\tilde{v}}$	= 2/3	$C_{\omega1}$	= $\frac{C_{b1}}{\kappa^2} + \frac{1 + C_{b2}}{\sigma_{\tilde{v}}}$
C_{b1}	= 0.1355	$C_{\omega2}$	= 0.3
C_{b2}	= 0.0622	$C_{\omega3}$	= 2

2.3 Mesh and Boundary Conditions

In order to solve the compressible RANS equations, a three-dimensional, unstructured mesh was employed. As seen in Figure 3, the projectile's front, top, and bottom were each extended by a factor of three times its length and its rear by a factor of six times its length in the process of creating the computational domain. In order to ensure that the wall unit y^+ was less than 1, the first layer thickness was set to 1.25×10^{-6} , as illustrated in Figure 3. The entire computational domain comprised approximately 1.2 million cells. The domain was subjected to far-field boundary conditions at the inlet, bottom, and top boundaries. Additionally, the outlet boundary was defined as a pressure outlet.

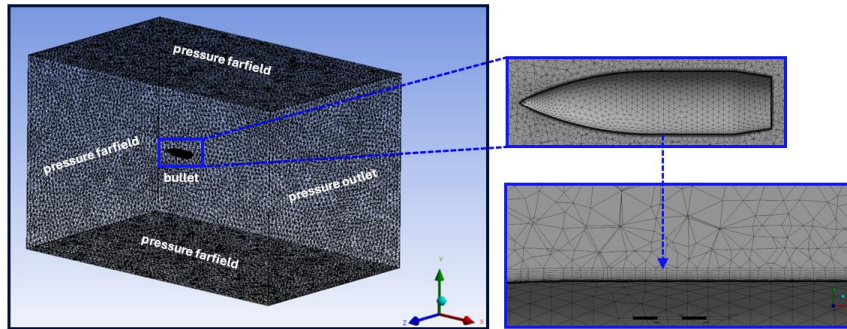


Figure 3. The schematic of the computational domain with boundaries and mesh structure

3 RESULTS AND DISCUSSION

Figure 4 presents a planar section depicting the Mach number contours for various bullet types. As expected, the flow exhibited axisymmetric characteristics for all examined projectiles. When the figures were examined, the subsonic stagnation zone and the corresponding velocity drop upstream of the nose tip were noticeable. The lower Mach number flow region ahead of the nose tip resulted from the flow's anticipation of the bullet's presence, as the flow remained subsonic. The flow reached a speed slightly exceeding the speed of sound as it expanded around the ogive nose and once again at the point where the boattail meets the rest of the object. Additionally, the presence of expansion fans and recompression shocks were observed at the ogive-body transition, the boattail-body transition, and the projectile base.

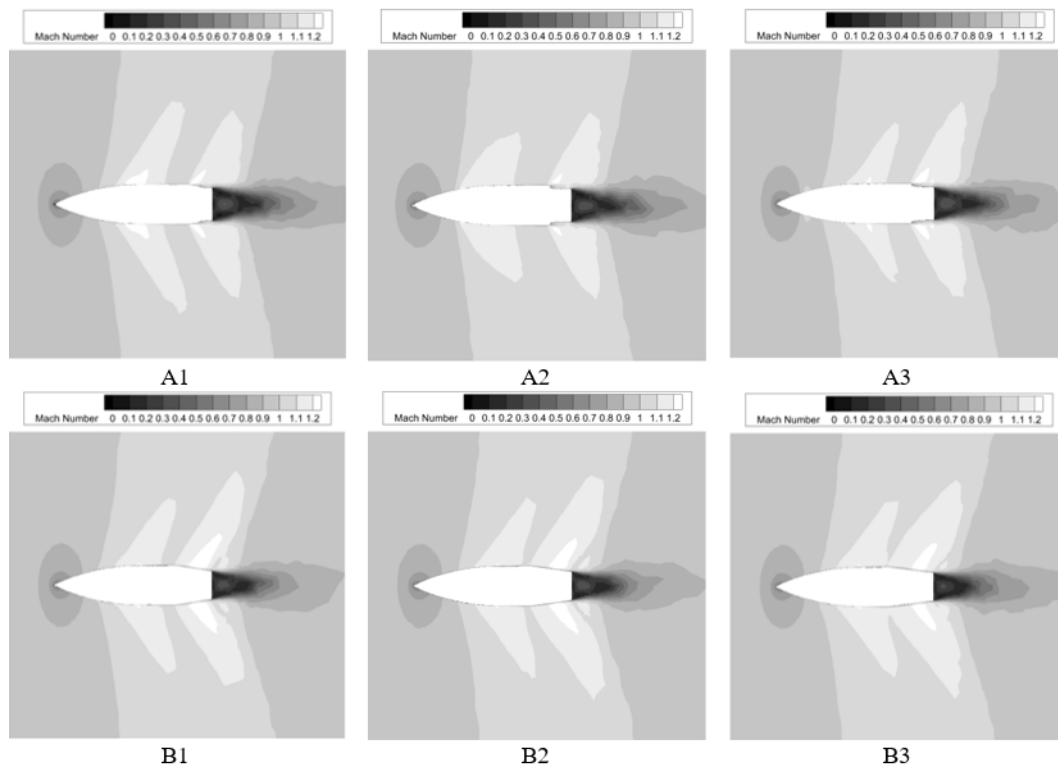


Figure 4. Mach number distribution around the bullets

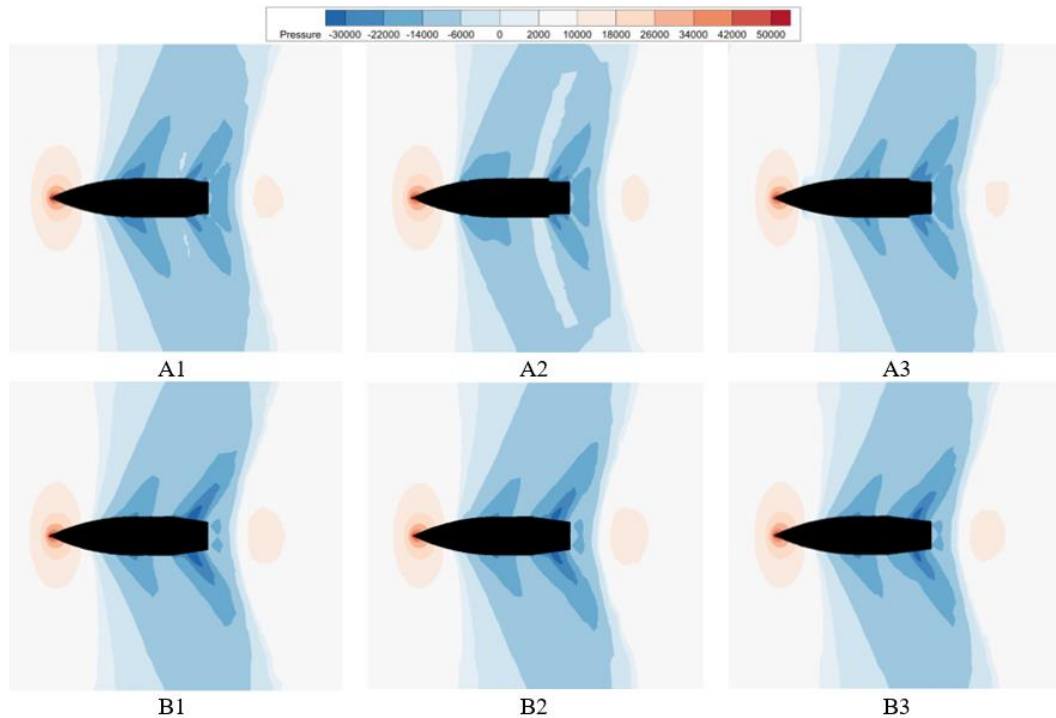


Figure 5. Pressure distribution around the bullets

Figure 5 displays a two-dimensional section that shows pressure contours for bullets with helical (A series) and straight grooves (B series). It was deduced that the pressure distribution across the central portion of the bullet was nearly symmetrical. Looking at the front pressure regions, both A-series and B-series bullets had high pressure regions at the front, indicating that the initial impact with the air was similar for both helical and straight groove designs. Also, in the side and rear pressure distributions, the low-pressure regions were more extensive and intense in the B-series (straight grooves) compared to the A-series (helical grooves). This suggests that straight grooves may cause more pronounced flow separation and turbulence.

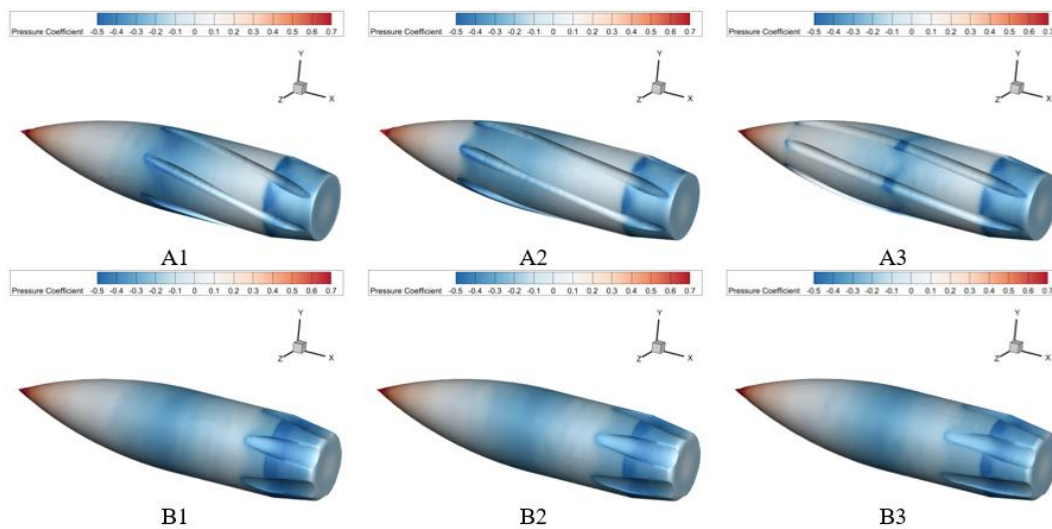


Figure 6. The distribution of pressure coefficient on surface of bullets

The pressure coefficient (C_p) distribution on a projectile is an important parameter for understanding the projectile's flight characteristics and aerodynamic performance. The aforementioned study analyzed the 3D distribution of pressure coefficients on the projectile, as shown in Figure 6. It is revealed that as the projectile advances, it compresses the surrounding air, thereby subjecting the noses of all bullets to high-pressure conditions. With the deceleration of the air hitting the projectile tip, the pressure increased, and naturally, the pressure coefficient value reached its maximum value of $C_p= 0.7$. As the projectile transitioned from the nose to the body, the pressure coefficient dropped to $C_p= -0.5$. We observed a gradual decrease in pressure along the projectile surface as the flow around it stabilized. This resulted in a more consistent and lower pressure coefficient compared

to the nose. The pressure coefficient significantly decreased in the rear part of the projectile, forming a low-pressure region. This region frequently exhibits the phenomenon of flow separation and turbulence, which results in increased drag.

Figure 6 shows a bar chart comparing the results of the drag coefficient (C_d) of different bullet types obtained from the numerical analysis, including those with helical grooves (A series) and straight grooves (B series), as well as a standard bullet without grooves. The effectiveness of grooves was examined, and it was found that the A series generally exhibited a lower drag coefficient than the B-series and the standard bullet. Among the A series, A2 and A3 exhibited the lowest C_d , indicating the most significant reduction in drag. In contrast, the B series also demonstrated reduced drag compared to the standard bullet, with B1 exhibiting the lowest C_d in the B series. The results demonstrated that A-series were more effective in reducing the drag coefficient than straight grooves. The gradual decrease in C_d from A1 to A3 indicated that the effectiveness of the helical grooves improved with the specific design or configuration used in A2 and A3. In contrast, B-series also contributed to reducing the drag coefficient, but not to the same extent as helical grooves. The C_d values for B1, B2, and B3 were relatively similar, indicating a reduced degree of variation in performance due to the straight grooves. The highest C_d value indicates that the standard bullet without grooves experiences the most drag, confirming that both helical and straight grooves enhance aerodynamic performance.

As a conclusion, helical grooves demonstrated the most significant reduction in drag, with A3 being the most effective performer. The lowest value of C_d was found to be 0.288 in the A3-type bullet, which has the geometry with the longest length of the spiral groove formed on the bullet. This resulted in an improvement of 12.4% in drag compared to the original bullet. In addition, B-series demonstrated a moderate reduction in drag compared to the standard bullet. Enhancing aerodynamic performance by managing flow separation at the tail was not as effective as helical grooves. Conversely, the standard bullet exhibited the highest drag, indicating the advantage of incorporating grooves into bullet design for improved performance. For applications where minimizing drag is crucial, the A-series bullets, particularly A2 and A3, would be the optimal choice. The B-series bullets continued to demonstrate improvements over the standard design and could be considered where simpler manufacturing or other design constraints are a factor.

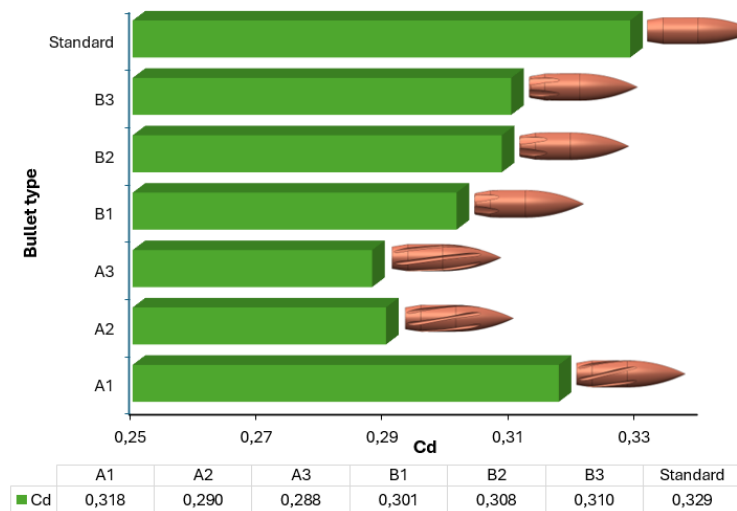


Figure 7. The variations in drag coefficients for all types of bullets

4 CONCLUSION

The aim of this study was to reduce the drag coefficients by modifying the shape of the Spitzer-type ogive bullet and analyzing the flow conditions, Mach number, and pressure distributions around the bullet through a three-dimensional numerical simulation. After analyzing the results, it was noted that the flow displayed areas of subsonic stagnation and a decrease in velocity before reaching the tip of the nose. The flow reached a speed slightly faster than the speed of sound as it expanded around the ogive nose and the junction where the boat-shaped tail meets the body. Expansion fans and recompression shocks were detected at the points where the ogive-shaped nose of the bullet meets the body, where the boattail-shaped rear of the bullet meets the body, and at the base of the bullet. The 3D spatial arrangement of pressure coefficients on the bullet indicates that as the bullet moves forward, it compresses the air in its vicinity, resulting in high-pressure conditions on the bullet tips. The pressure coefficient reached its peak at $C_p=0.7$ when the air slowed down and decreased to $C_p=-0.5$ as the projectile moved from the front to the main part. The pressure coefficient on the projectile surface exhibited a consistent and lower

value due to a gradual decrease in pressure. The numerical analysis indicated that helical grooves significantly reduced drag, with A3 being the most effective performer. The A3-type bullet, with the longest spiral groove, improved drag by 12.4% compared to the original bullet. B-series showed a moderate reduction in drag. However, managing flow separation at the tail was not as effective as helical grooves. The standard bullet had the highest drag, indicating the advantage of incorporating grooves into bullet design. A-series bullets, particularly A2 and A3, were ideal for applications requiring minimal drag. B-series bullets showed improvements over the standard design and could be considered for simpler manufacturing or design constraints.

Acknowledgments

The authors would like to thank TUBITAK (The Scientific and Technological Research Council of Turkey) (Project number: 2209-A-1919B012109748) for their financial support.

Author Contributions

Hacimurat DEMİR: Conceptualization, Methodology, Software, Formal analysis, Writing - Original Draft, Writing - Review & Editing, Visualization, Supervision

Mehmet ÇİMEN: Software, Investigation, Resources

Ömer YILMAN: Investigation, Validation

Erhan TEKİN: Investigation

All authors read and approved the final manuscript.

Conflict of interest

No conflict of interest was declared by the authors.

References

- [1] R. L. McCoy, *Modern Exterior Ballistics*. Schiffer Military History, 2012.
- [2] A. Ferfour, T. Allouche, D. D. Jerković, N. Hristov, M. Vučković, and A. Benmeddah, "Prediction of drag aerodynamic coefficient of the 155mm projectile under axisymmetric flow using different approaches," *Journal of the Serbian Society for Computational Mechanics*, vol. 17, no. 2, pp. 69–86, Dec. 2023.
- [3] S. Sahoo and M. K. Laha, "Coefficient of Drag and Trajectory Simulation of 130 mm Supersonic Artillery Shell with Recovery Plug or Fuze," *Defence Science Journal/Defence Science Journal*, vol. 64, no. 6, pp. 502–508, Nov. 2014.
- [4] T. Gholap, R. Salokhe, G. Ghadage, S. Mane, and D. Sahoo, "Aerodynamic analysis of an AK-47 bullet moving at mach 2.0 in close proximity to the ground," *FME Transactions*, vol. 50, no. 2, pp. 369–381, Jan. 2022.
- [5] S. Selimli, "Yüzey geometrisinin mermi aerodinamik davranışları üzerine etkisinin nümerik incelenmesi," *Politeknik Dergisi*, 24(1), 299-304, 2021.
- [6] D. S. K. Reddy, P. K. Sah, and A. Sharma, "Prediction of Drag Coefficient of a Base Bleed Artillery Projectile at Supersonic Mach number," *Journal of Physics. Conference Series*, vol. 2054, no. 1, p. 012013, Oct. 2021.
- [7] A. Khan, I. Shah, S. Aziz, M. Waqas, U. K. U. Zaman, and D.-W. Jung, "Numerical and Experimental Analysis of Drag and Lift Forces on a Bullet Head," *Aerospace*, vol. 9, no. 12, p. 816, Dec. 2022.
- [8] C. Gan "Computational Fluid Dynamics (CFD) of Drag Force for Bullet's Shape Design." In *Journal of Physics: Conference Series* , Vol. 1888, No. 1, p. 012016
- [9] S. Salunke, S. Shinde, T. Gholap, and D. Sahoo, "Comparative computational analysis of NATO 5.56 mm, APM2 7.62 mm and AK-47 7.82 mm bullet moving at Mach 2.0 in close vicinity to the wall," *FME Transactions*, vol. 51, no. 1, pp. 81–89, Jan. 2023.
- [10] S. Serdarevic-Kadic and J. Terzic, "Effects of Base Shape to Drag at Transonic and Supersonic Speeds by CFD," in *DAAAM international scientific book*, pp. 071–080, 2019.
- [11] B. Litz, *Applied Ballistics for Long-Range Shooting*, 2nd ed., Applied Ballistics LLC, 2011.
- [12] Larson, E., Lwali, R., & Samardzic, D. (2015). Bullet drag estimation with compressible conical flow equations and commercial software. *Department of Aerospace Engineering and Engineering Mechanics, San Diego State University research*.

- [13] I. Asproulias, "RANS modelling for compressible turbulent flows involving shock wave boundary layer interactions," PhD Thesis, UK: The University of Manchester, 2014.
- [14] <https://www.afs.enea.it/project/neptunius/docs/fluent/html/th/node421.htm> [Online]. Available, [Accessed: 31-May-2024].
- [15] P. Spalart and S. Allmaras, "A one-equation turbulence model for aerodynamic flows," *30th Aerospace Sciences Meeting and Exhibit*, Jan. 1992.